Mathematical Biology

CrossMark

Receptor heterogeneity in optical biosensors

Ryan M. Evans[1] · **David A. Edwards[2]**

Abstract Scientists measure rate constants associated with biochemical reactions in an optical biosensor—an instrument in which ligand molecules are convected through a flow cell over a surface to which receptors are immobilized. We quantify transport effects on such reactions by modeling the associated convection-diffusion equation with a reaction boundary condition. In experimental situations, the full PDE model reduces to a set of unwieldy integrodifferential equations (IDEs). Employing common physical assumptions, we may reduce the system to an ODE model, which is more useful in practice, and which can be easily adapted to the inverse problem of finding rate constants. The results from the ODE model compare favorably with numerical simulations of the IDEs, even outside its range of validity.

✉ Ryan M. Evans
  ryan.evans@nist.gov

  David A. Edwards
  dedwards@udel.edu

[1] Applied and Computational Mathematics Division, Information and Technology Laboratory, National Institute of Standards and Technology, 100 Bureau Drive, Gaithersburg, MD 20899, USA

[2] Department of Mathematical Sciences, University of Delaware, Newark, DE 19716, USA

1 Introduction

Many biochemical reactions involve a stream of chemical reactants (*ligand molecules*) flowing through a fluid-filled volume, and another reactant (the *receptor*) confined to a surface. Such *surface-volume* reactions occur during platelet adhesion (Austin 2009), drug absorption (Bertucci et al. 2007), antigen–antibody interactions (Raghaven et al. 1994), and DNA damage repair (Zhuang et al. 2008). Fundamental to understanding these reactions is getting accurate quantitative measurements of the underlying reaction rate constants. To measure rate constants associated with surface-volume reactions, scientists use *optical biosensors*: see Fig. 1 for a schematic of one such instrument.

The first step of any biosensor experiment is to immobilize receptors on the sensor surface. This is done by injecting receptors into the biosensor in a buffer fluid, and letting them diffuse through the buffer onto the channel floor to bind with molecules already confined to the surface. We note that this process is itself a surface-volume reaction.

After receptors are deposited onto the surface, chemists inject ligand molecules into the biosensor in the buffer—this is the *injection phase*. Ligand molecules are transported through the buffer onto the channel floor to bind with the immobilized receptors. During this process, an evanescent wave reflects off the channel floor and passes to a detector which measures refractive changes on the surface due to ligand binding. In particular, let $B(x, t)$ denote the concentration of bound ligand molecules. Then the refractive changes are averaged of a portion of the channel floor $[x_{\min}, x_{\max}]$ to produce real-time feedback in the form of a *sensogram reading*
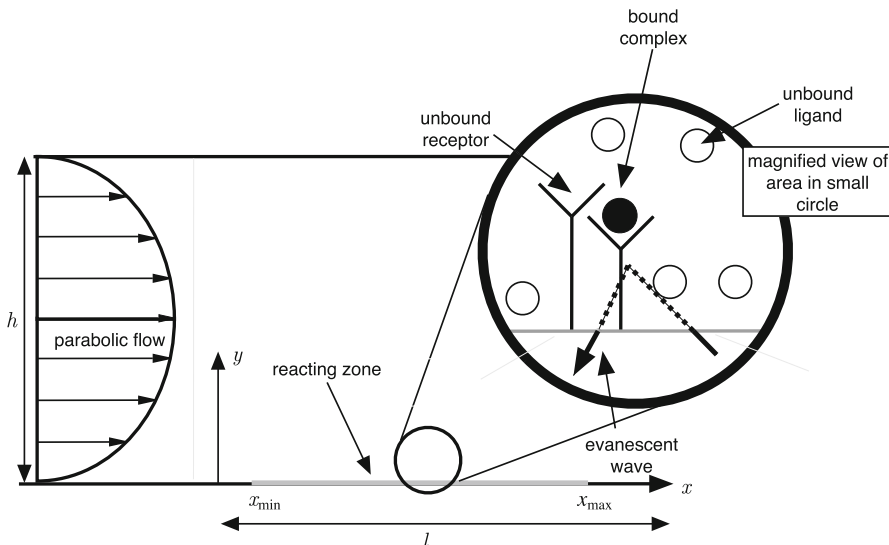
Fig. 1 Cross-sectional schematic of binding/unbinding in an optical biosensor. Ligand molecules are injected into the biosensor, and diffuse to bind with receptor sites on the surface. Mass changes on the surface due to ligand binding are averaged over $[x_{\min}, x_{\max}]$ to produce measurements of the form (1.1a)

$$S(t) = s\,\overline{B}(t), \tag{1.1a}$$

$$\overline{B}(t) = \frac{1}{x_{\max} - x_{\min}} \int_{x_{\min}}^{x_{\max}} B(x, t)\,\mathrm{d}x. \tag{1.1b}$$

Note that even though we are using the standard bar notation for average quantities, we are not averaging over the whole floor; just the subset $[x_{\min}, x_{\max}]$ scanned by the device (Edwards 1999). In (1.1a), s is proportional to the molecular weight of the ligand.

After the bound state concentration reaches a chemical equilibrium, scientists prepare the device for another experiment by washing it with the buffer—this is the *wash phase* of the experiment. Only pure buffer is flowing through the biosensor during the wash phase, not buffer containing the ligand molecules. This has the effect of causing all of the bound ligand molecules at the surface to dissociate, thereby preparing the device for another experiment.

Biosensor technology has become extremely popular in recent years. Rich observes in Rich and Myszka (2011) that 10,000 papers have cited the use of an optical biosensor as of 2009 alone. Since interpreting biosensor data relies on a mathematical model, models for biosensor experiments have been proposed and studied. Edwards et al. quantify boundary layer transport effects on unimolecular reactions in Edwards (1999), Edwards et al. (1999); the effects of a dextran gel layer in Edwards (2001); and arrays of reacting zones in Edwards (2011), Zumbrum and Edwards (2014). Effects of signal decay associated with the measuring wave were studied in Edwards (2004), Liedberg et al. (1993), Schuck (1996) by Edwards, Liedberg et al., and Schuck respectively. Gervais and Jensen study mass transport and surface reactions in microfluidic systems in Gervais and Jensen (2006), with a particular emphasis on the transport-limited parameter regime. In Goldstein et al. (1999), Goldstein and coworkers identify conditions under which transport procceses have a negligible effect on reaction kinetics, and propose a spatially homogenous two-compartment model for when transport effects must be taken into account. Lagrée conducts a comparison of simplified models of microfluidic surface reacting flows in Lagrée and Ivan-Fernolendt (2004). Jenkins and coworkers take a computational approach in Jenkins et al. (2004), by solving a Partial differential Equation (PDE) model for protein adsorption in a microfluidic system with computational fluid dynamics software. In Myszka et al. (1998) Myszka uses a combination of numerical simulations and physical experiments to determine the accuracy of a spatially homogeneous two-compartment model (similar to the one proposed in Goldstein et al. (1999)), and in Rich et al. (2008) Rich and Myszka extend this work to systems with arrays of reacting zones. Hu and coworkers model and numerically study the effects of an electrokinetically driven microfludic flow on surface-volume reactions in Hu et al. (2007).

Although the aforementioned models are limited to the presence of only a single reacting species, many biochemical processes involve multiple interacting components. One example of such a multiple-component process occurs during DNA damage repair. In order to cope with harmful DNA lesions, cells engage in a process known as DNA translesion synthesis. This process is described in great detail elsewhere (Friedberg 2005; Lehmann et al. 2007; Plosky and Woodgate 2004). For our purposes it
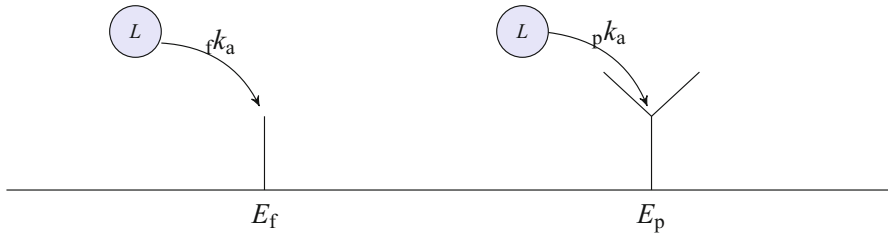
Fig. 2 A ligand molecule binding with a free DNA receptor E_f and with a PCNA receptor E_p

is sufficient to know that DNA translesion synthesis involves three interacting components: a Proliferating Cell Nuclear Antigen (PCNA) molecule, polymerase δ, and polymerase η. Moverover, in order for a successful DNA translesion synthesis event to occur, polymerase δ must bind with a PCNA molecule. A central question surrounding DNA translesion synthesis is whether the PCNA and polymerase δ complex forms as a result of direct binding, or a ligand switching process. The latter involves the two polymerase molecules (the ligands) trading places on a PCNA molecule (the receptor). In Evans and Edwards (2017), the authors study the polymerase switch by modeling the associated *multiple-ligand* biosensor experiment with only a single type of receptor on the reacting surface (i.e., the PCNA molecule). On the other hand, it has been hypothesized that there are in fact *two receptor types* present during such biosensor experiments: the PCNA molecules, and free DNA molecules.

Such heterogeneous receptor populations result from the receptor immobilization phase of biosensor experiments. During this phase, scientists seek to deposit PCNA molecules onto free DNA molecules already confined to the sensor surface. Although scientists seek to saturate the sensor surface with PCNA molecules, not every single free DNA molecule confined to the surface may be paired with a PCNA molecule, so at the start of the injection phase there may be both free DNA receptors and free DNA receptors with a PCNA molecule attached (henceforth we shall refer to the latter as simply PCNA receptors). It follows that ligand molecules can bind with either free DNA receptors or PCNA molecules during the experiment. These reactions are shown in Figs. 2 and 3, and stated precisely as

$$E_f + L \underset{_fk_d}{\overset{_fk_a}{\rightleftharpoons}} E_fL, \tag{1.2a}$$

$$E_p + L \underset{_pk_d}{\overset{_pk_a}{\rightleftharpoons}} E_pL. \tag{1.2b}$$

In our notation L denotes a ligand molecule, E_f denotes a free DNA receptor, E_p denotes a PCNA receptor, $_fk_a$ denotes the rate at which a ligand molecule binds with a free DNA receptor, and $_fk_d$ denotes the rate at which a ligand molecule dissociates from a free DNA receptor; the parameters $_pk_a$ and $_pk_d$ have similar interpretations.

We explore the single-receptor assumption made by the authors in Evans and Edwards (2017) by modeling the multiple-receptor reactions (1.2). Though we have the afforementioned application in mind, the model presented herein is general and
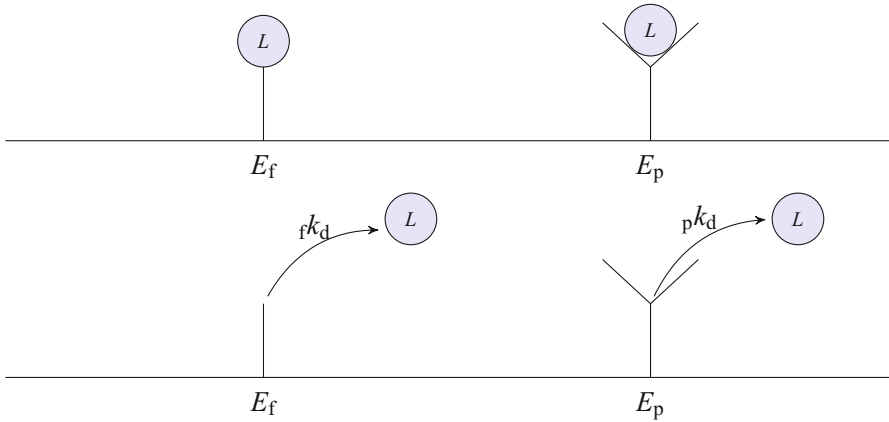
Fig. 3 *Above* a ligand molecule bound to a free DNA receptor E_f and to a PCNA receptor E_p. *Below* a ligand molecule dissociating from a free DNA receptor E_f and a PCNA receptor E_p

multiple-receptor reaction kinetics is an experimentally relevant topic (Cooper 2009, pp. 112–113; O'Shannessy 1994; O'Shannessy and Winzor 1996; Schuck 1997) that has received little attention to date. To mathematically account for multiple receptor types researchers commonly apply the well-stirred approximation, in which reaction kinetics decouple from transport effects. In this case, the governing equations reduce to a simple set of Ordinary Differential Equations (ODEs). Unfortunately this decoupling is accurate only inside a narrow parameter range, outside of which mass transport effects influence kinetic rate constant measurements. Indeed, the experimental relevance of mass transport effects is well known (Balgi et al. 1995; Glaser 1993; Myszka et al. 1998).

Svitel et al. attempt to quantify mass transport effects on ligand binding in the presence of a heterogeneous receptor population in Svitel et al. (2007). In this manuscript, the authors consider a continuous distribution of functionally distinct and independent receptor sites, which they ultimately discretize to a finite number of N different receptors. Moreover, they account for mass transport effects through a two-compartment model, in which each compartment is assumed to be internally well-mixed and spatially homogeneous [similar to the approaches proposed in Goldstein et al. (1999), Myszka et al. (1998), Rich et al. (2008)]. This assumption reduces the governing equations in each compartment to a set of ODEs. We consider a more sophisticated model of transport in the present work by modeling the experiment with a convection-diffusion equation with a reaction boundary. Given that mass transport effects and receptor heterogeneity are the two most common reason why theoretical predictions deviate from experimental data (Schuck and Zhao 2010), our approach has the advantage of rigorously quantifying transport processes during multiple-receptor biosensor experiments, thereby giving researchers a precise and efficient tool for measuring kinetic rate constants.

The rest of the paper is organized as follows. In Sect. 2, we present the full PDE model and show how this model simplifies to a set of nonlinear IDEs. In Sect. 3.1, we show the latter further reduces to a set of nonlinear ODEs. In Sect. 3.2, we present a

numerical method for solving our IDE system. We verify the accuracy of the reduction from the IDE system to the ODE system in Sect. 3.3, where we demonstrate that the two solutions agree for a wide parameter range. Conclusions and plans for future work are discussed in Sect. 4.

2 Governing equations

In this section we model the kinetics system (1.2). Since the multiple-receptor model presented herein has not been considered before, we present the governing equations in complete detail. To introduce our model we let $\mathbf{B}(x, t) = (B_p(x, t), B_f(x, t))^T \in \mathbb{R}^2$ be a vector containing the concentration of ligand bound to a PCNA receptors $B_p(x, t)$, and free DNA receptors $B_f(x, t)$. We begin with the injection phase of the experiment by applying the law of mass action to (1.2) to find

$$\frac{\partial B_p}{\partial t} = {}_p k_a (R_p - B_p) C(x, 0, t) - {}_p k_d B_p, \tag{2.1a}$$

$$\frac{\partial B_f}{\partial t} = {}_f k_a (R_f - B_f) C(x, 0, t) - {}_f k_d B_f, \tag{2.1b}$$

$$\mathbf{B}(x, 0) = \mathbf{0}, \tag{2.1c}$$

where R_p and R_f denote the initial concentration of available PCNA and free DNA receptors, and $C(x, y, t)$ denotes the unbound ligand concentration. In addition, we let

$$R_t = R_p + R_f \tag{2.2}$$

be the total initial receptor concentration. The set of Eqs. (2.1) holds on the reacting surface when $y = 0$ and $x \in [0, l]$. Here l denotes the length of the biosensor, which is much greater than its height h—the aspect ratio $\varepsilon = h/l$ is small.

Though these equations appear to decouple, we shall see the coupling enters through the diffusive flux condition

$$D \frac{\partial C}{\partial y}(x, 0, t) = \frac{\partial B_\Sigma}{\partial t}(x, t), \tag{2.3a}$$

for $x \in [0, l]$ and $y = 0$. In (2.3a) D is the diffusion coefficient of the ligand L, and $B_\Sigma(x, t) = B_p(x, t) + B_f(x, t)$. This equation states that the diffusive flux *into* the surface (hence the positive sign) is used up in the reaction. In addition, we remark that the receptors obviously have finite height and so the reaction strictly occurs in a thin reacting zone above $y = 0$. However, it can be shown that the height of this zone is negligible, and hence we may replace the reacting zone with the flat surface at $y = 0$ (Edwards 2006a, b).

In the channel $C(x, y, t)$ obeys a standard convection equation with a Poisieulle flow profile

$$\frac{\partial C}{\partial t} = D \nabla^2 C - \mathbf{v} \cdot \nabla C, \qquad \mathbf{v} = \left(\frac{V y}{h} \left(1 - \frac{y}{h} \right), 0 \right), \tag{2.3b}$$

for $(x, y) \in (0, l) \times (0, h)$ and $t > 0$. Here V is the characteristic velocity associated with our flow. There is initially no unbound ligand in the channel

$$C(x, y, 0) = 0. \tag{2.3c}$$

After $t > 0$, ligand is injected into the channel at a uniform concentration

$$C(0, y, t) = C_u. \tag{2.3d}$$

A no-flux condition holds on the ceiling

$$\frac{\partial C}{\partial y}(x, H, t) = 0. \tag{2.3e}$$

Furthermore, the reacting zone doesn't extend to the end of the channel, so the concentration equilibrates by the time it exits the channel

$$\frac{\partial C}{\partial x}(L, y, t) = 0. \tag{2.3f}$$

The presence of multiple receptor types on the surface changes the form of biosensor feedback. The sensogram reading (1.1a) now takes the form

$$S(t) = s \, \overline{B}_f(t) + s \, \overline{B}_p(t) = s \, \overline{B}_\Sigma(t), \tag{2.4a}$$

$$\overline{B}_j(t) = \frac{1}{x_{max} - x_{min}} \int_{x_{min}}^{x_{max}} B_j(x, t) \, dx, \tag{2.4b}$$

where the index j can equal p, f, or Σ. Observe that since the sensogram reading is proportional to only the sum of the reacting species—not the individual reacting species themselves—fitting the four kinetic rate constants in (1.2) directly to the signal (2.4a) could lead to erroneous measurements, since different sets of rate constants could lead to similar sensogram mass readings. Hence, in Sect. 3.1 we propose an experimental design protocol for identifying the true set of rate constants (Table 1).

Edwards has shown that due to high Péclet number flow, transport effects are relevant only in a thin unstirred layer near the surface (Edwards et al. 1999); thus, the relevant dimensionless variables are

$$\widetilde{B}_p = \frac{B_p}{R_t}, \quad \widetilde{B}_f = \frac{B_f}{R_t}, \quad \widetilde{B}_\Sigma = \frac{B_\Sigma}{R_t}, \quad \widetilde{\mathbf{B}} = \left(\frac{B_p}{R_t}, \frac{B_f}{R_t}\right)^T, \quad \widetilde{C} = \frac{C}{C_u}, \quad \widetilde{t} = {}_f k_a C_u \, t,$$

$$\widetilde{x} = \frac{x}{l}, \quad \widetilde{y} = \frac{y}{h}, \quad \widetilde{\eta} = Pe^{1/3} y, \quad Pe = \frac{V h^2}{D l}, \quad {}_p \widetilde{K}_a = \frac{{}_p k_a}{{}_f k_a}, \quad {}_p \widetilde{K}_d = \frac{{}_p k_d}{C_u \cdot {}_f k_a},$$

$$ {}_f \widetilde{K}_a = \frac{{}_f k_d}{C_u \cdot {}_f k_a}. \tag{2.5}$$

Table 1 Bounds for dimensional parameters are listed below

Parameter	Description	Range	References
Dimensional parameters			
D (cm^2/s)	Diffusion coefficient	4×10^{-7}	Torre et al. (2000)
$^{f}k_a$ (cm^3/(mol s))	Association rate constant in (1.2a)	10^3–3×10^9	BIAcore T200 data file (2013), Rich et al. (2008), Yarmush et al. (1996)
$^{f}k_d$ (s^{-1})	Dissociation rate constant in (1.2a)	10^{-5}–1	BIAcore T200 data file (2013), Rich et al. (2008), Yarmush et al. (1996)
$^{p}k_a$ (cm^3/(mol s))	Association rate constant in (1.2b)	10^3–3×10^9	BIAcore T200 data file (2013), Rich et al. (2008), Yarmush et al. (1996)
$^{p}k_d$ (s^{-1})	Dissociation rate constant in (1.2b)	10^{-5}–1	BIAcore T200 data file (2013), Rich et al. (2008), Yarmush et al. (1996)
h (cm)	Biosensor length	0.05	Rich et al. (2008)
l (cm)	Biosensor height	2	Rich et al. (2008)
w (cm)	Biosensor width	1.3	Rich et al. (2008)
R_t (mol/cm^2)	Total receptor concentration	1.11×10^{-13}–2.33×10^{-11}	Rich et al. (2008), Yarmush et al. (1996)
V (cm/s)	Characteristic velocity	0.001–2.88	BIAcore T200 data file (2013), Rich et al. (2008), Yarmush et al. (1996)
C_u (mol/s)	Ligand inflow concentration	2.96×10^{-12}–2×10^{-10}	Rich and Myszka (2011)
ν (cm^2/s)	Kinematic viscosity	10^{-2}	Bird (2002)

As experimental data is still forthcoming, for the kinetic rate constants we have listed extremal bounds from the literature. The characteristic velocity V was calculated from flow rates in the given references using the formula $V = 6Q/(wh)$ derived in Edwards (2011). Per convention, the parameter ν denotes the kinematic viscosity of water at 20 °C, and is not related to the convolution variable used throughout

Observe that we have scaled the bound ligand concentrations B_f and B_p by the total receptor concentration R_t (2.2). Physically, the free DNA molecules confined to the sensor surface should be nearly saturated with PCNA molecules by the end of the receptor immobilization phase, so we expect the ratio of the free DNA receptor concentration R_f to the total receptor concentration R_t to be small; i.e., $\widetilde{R}_f = R_f/R_t \ll 1$. Similarly, we may define $\widetilde{R}_p = R_p/R_t$, so that $\widetilde{R}_f + \widetilde{R}_p = 1$.

In addition, we nondimensionalize the sensogram reading (2.4a) by setting

$$\widetilde{S}(\widetilde{t}) = \frac{S}{s\,R_t} = \frac{1}{\widetilde{x}_{\max} - \widetilde{x}_{\min}} \int_{\widetilde{x}_{\min}}^{\widetilde{x}_{\max}} \widetilde{B}_f(\widetilde{x}, \widetilde{t})\,d\widetilde{x} + \frac{1}{\widetilde{x}_{\max} - \widetilde{x}_{\min}} \int_{\widetilde{x}_{\min}}^{\widetilde{x}_{\max}} \widetilde{B}_p(\widetilde{x}, \widetilde{t})\,d\widetilde{x}.$$
(2.6)

We use the values $\widetilde{x}_{\min} = 0.2$ and $\widetilde{x}_{\max} = 0.8$ in our numerical simulations [see (Edwards 1999) for a unified table of experimental values from the literature]. *Henceforth, we drop the tildes on our dimensionless variables for simplicity.* In particular, from now on we shall use (2.4b) to denote the *dimensionless* average concentrations $\overline{B}_j(t)$, for $j = p$, f, or Σ.

Our new independent variables t, η, and x are the boundary layer coordinates. Indeed, high Péclet number flow implies that convection dominates everywhere except a thin region near the surface, in which convection and diffusion balance. Hence, to study reaction in the boundary layer, in (2.5) we have scaled y with the boundary layer width of $Pe^{1/3}$ and time with the reaction rate $_f k_a C_u$. A more detailed discussion of these scalings is found in Edwards (1999).

In terms of the dimensionless variables (2.5), the system (2.1) is

$$\frac{\partial B_p}{\partial t} = {}_pK_a(R_p - B_p)C(x, 0, t) - {}_pK_d B_p,$$
(2.7a)

$$\frac{\partial B_f}{\partial t} = (R_f - B_f)C(x, 0, t) - {}_fK_d B_f,$$
(2.7b)

$$\mathbf{B}(x, 0) = \mathbf{0}.$$
(2.7c)

The dimensionless diffusive flux condition is given by

$$\frac{\partial C}{\partial \eta}(x, 0, t) = \mathrm{Da}\frac{\partial B_\Sigma}{\partial t}.$$
(2.8)

The parameter Da on the right hand side of (2.8) is the Damköhler number. In terms of raw parameters Da is given by

$$\mathrm{Da} = \frac{{}_f k_a R_t (hl)^{1/3}}{(V D^2)^{1/3}}.$$
(2.9)

The two experimentally relevant cases are $\mathrm{Da} \ll 1$ and $\mathrm{Da} = O(1)$. When $\mathrm{Da} \ll 1$, the speed at which ligand molecules are transported to the surface is much faster than reaction. Hence the rate at which the bound state concentrations $B_p(x, t)$ and $B_f(x, t)$ evolve is limited by the intrinsic reaction rate, and we refer to this parameter

regime as the reaction-limited regime. Conversely, when $\mathrm{Da} = O(1)$, transport into the surface and reaction proceed at the same rate. In this case, the evolution of $B_\mathrm{p}(x, t)$ and $B_\mathrm{f}(x, t)$ depends upon both the speed of reaction and transport processes. It is for these reasons that scientists seek to design biosensor experiments so that $\mathrm{Da} \ll 1$, because in this case reaction and diffusion occur on different time scales and one is in a better position to measure reaction rate constants (Edwards et al. 1999).

In the boundary layer (2.3b) reduces to

$$\frac{\partial^2 C}{\partial \eta^2} = \eta \frac{\partial C}{\partial x}, \tag{2.10a}$$

with the normalized inflow and matching conditions

$$C(0, \eta, t) = 1, \tag{2.10b}$$

$$\lim_{\eta \to \infty} C(x, \eta, t) = 1 \tag{2.10c}$$

for all t. Equation (2.10c) expresses the requirement that the concentration in the layer must match the uniform concentration of $C(x, y, t) = 1$ as one exits the layer.

Thus, in the boundary layer the bound state concentration is governed by (2.7), (2.8), and (2.10). To proceed, we need a closed form for $C(x, 0, t)$. First, we apply a Laplace transform in x to transform (2.10a) into an Airy's equation. Next, we use the fact that the derivative of the transformed solution is known at $\eta = 0$ to show

$$C(x, 0, t) = 1 - \frac{\mathrm{Da}}{3^{1/3} \Gamma(2/3)} \int_0^x B_\Sigma(x - v, t) \frac{\mathrm{d}v}{v^{2/3}}. \tag{2.10d}$$

For the interested reader, details of similar calculations may be found in Edwards et al. (1999), Evans and Edwards (2017). From (2.10d) we see that *transport effects* couple the reactions governed by (2.7). While (2.7) decouples in the well-stirred limit (when Da approaches zero), stronger transport effects drive up Da and result in a stronger coupling. Furthermore, the convolution integral reflects the phenomenon of upstream ligand depletion. At the start of the experiment, ligand molecules diffuse to the surface to bind with receptor sites upstream, before they diffuse to bind with receptor sites downstream.

We now present the dimensionless governing equations for the wash phase. By the time the wash phase starts, the bound state concentration will have reached a chemical equilibrium. However, the unbound ligand evolution occurs on a faster time scale than the bound state (Edwards 1999). Therefore, the initial condition for the wash phase is the solution to the steady state of (2.7a)–(2.7b) with $C(x, 0, t)$ replaced by the steady-state unbound concentration of 1

$$\mathbf{0} = -A\mathbf{B} + \mathbf{f}, \tag{2.11}$$

$$A = \begin{pmatrix} {}_\mathrm{p}K_\mathrm{a} + {}_\mathrm{p}K_\mathrm{d} & 0 \\ 0 & 1 + {}_\mathrm{f}K_\mathrm{d} \end{pmatrix}, \quad \mathbf{f} = (R_\mathrm{p} \cdot {}_\mathrm{p}K_\mathrm{a}, R_\mathrm{f})^T. \tag{2.12}$$

The solution of this linear system is

$$\mathbf{B}(x, 0) = A^{-1}\mathbf{f} = \left(\frac{R_\mathrm{p} \cdot {}_\mathrm{p}K_\mathrm{a}}{{}_\mathrm{p}K_\mathrm{a} + {}_\mathrm{p}K_\mathrm{d}}, \frac{R_\mathrm{f}}{1 + {}_\mathrm{f}K_\mathrm{d}} \right)^T. \tag{2.13}$$

Reaction kinetics during the wash phase are therefore governed by (2.7a)–(2.7b) with (2.13) as the initial condition. The diffusive flux condition (2.8) still holds, and the unbound ligand evolution is governed by (2.10a), with the inflow and matching conditions

$$C(0, \eta, t) = 0, \tag{2.14a}$$

$$\lim_{\eta \to \infty} C(x, \eta, t) = 0. \tag{2.14b}$$

Equation (2.14a) reflects the fact that no ligand is flowing into the biosensor during the wash phase, while (2.14b) reflects the fact that the unbound ligand concentration must match the concentration zero as one exits the layer; they both hold for all t. Similarly to how we derived (2.10d), one can use (2.8), (2.10a), and (2.14) to show that during the wash phase

$$C(x, 0, t) = -\frac{\mathrm{Da}}{3^{1/3}\Gamma(2/3)} \int_0^x \frac{\partial B_\Sigma}{\partial t}(x - \nu, t) \frac{\mathrm{d}\nu}{x^{2/3}}. \tag{2.15}$$

Again, the coupling is due to transport effects. The convolution integral in (2.15) captures the phenomenon of ligand rebinding: ligand molecules dissociating upstream may rebind to receptor sites further downstream. We note that since $B_\mathrm{p}(x, t)$ and $B_\mathrm{f}(x, t)$ are monotonically decreasing in time during the wash phase, $C(x, 0, t)$ is nonnegative. Additionally, the sensogram reading during the wash phase is still given by (2.6).

3 Effective rate constant approximation and verification

3.1 Effective rate constant equations

Despite its wide applicability, the IDE system derived in Sect. 2 is not typically used for parameter estimation. In practice, one typically makes the assumption that transport effects and reaction kinetics are completely decoupled. The governing equations in this case are recovered in the limit that Da approaches 0 in (2.7a)–(2.7b), using (2.10d) or (2.15). During the injection phase, these equations take the form

$$\frac{\mathrm{d}B_\mathrm{p}}{\mathrm{d}t} = {}_\mathrm{p}K_\mathrm{a}(R_\mathrm{p} - B_\mathrm{p}) - {}_\mathrm{f}K_\mathrm{d}B_\mathrm{p}, \tag{3.1a}$$

$$\frac{\mathrm{d}B_\mathrm{f}}{\mathrm{d}t} = (R_\mathrm{f} - B_\mathrm{f}) - {}_\mathrm{f}K_\mathrm{a}B_\mathrm{f}, \tag{3.1b}$$

$$B_\mathrm{p}(0) = B_\mathrm{f}(0) = 0. \tag{3.1c}$$

Data obtained by solving the linear decoupled ODE system (3.1) is then used in an iterative algorithm to fit the solution of the linear ODE model to physical experimental data (Rich and Myszka 2009, pp. 97–99).

The well-stirred assumption is valid only when Da $\ll$ 1, and outside of this parameter regime the reduction from (2.7), (2.10d) to (3.1) is inappropriate. Even in the well-stirred limit one commits an $O(\text{Da})$ error by replacing (2.7), (2.10d) with (3.1). On the other hand, our IDE system (2.7), (2.10d) is hopeless to solve in closed form and finding a numerical solution requires carefully handling the singularity in the integrand of (2.10d) at $\nu = 0$. However, we do not need the full solution of (2.7), (2.10d) to compute the sensogram signal (2.6), since the signal is function only of the average quantities $\overline{B}_p(t)$ and $\overline{B}_f(t)$. Hence, we proceed by deriving a set of nonlinear ODEs directly in terms of $\overline{B}_p(t)$ and $\overline{B}_f(t)$. In what follows, we will be using the standard bar notation introduced in the introduction to denote the spatial average of a function over the interval $[x_{\min}, x_{\max}]$.

We begin with the injection phase of the experiment by spatially averaging (2.7a)–(2.7b), in the sense of (2.4b). Doing so we are immediately confronted with terms such as

$$\overline{B_p(x, t)C(x, 0, t)} = \overline{B_p(x, t)\left(1 - \frac{\text{Da}}{3^{1/3}\Gamma(2/3)}\int_0^x \frac{\partial B_\Sigma}{\partial t}(\nu, t)\frac{d\nu}{(x - \nu)^{2/3}}\right)}. \quad (3.2)$$

We approximate the nonlinear term (3.2) when Da $\ll$ 1; i.e., in the reaction-limited parameter regime in which ligand molecules are are transported to the surface at a faster rate than reaction. In this case one may write a perturbation series for $\mathbf{B}(x, t)$ of the form

$$\mathbf{B}(x, t) = \mathbf{B}^{(0)}(t) + \text{Da } x^{1/3}\, \mathbf{B}^{(1)}(t) + O(\text{Da}^2), \quad (3.3)$$

where the factor of $x^{1/3}$ comes from the convolution integral. Substituting (3.3) into (2.7) using (2.10d), we note that to leading order $C = 1$ and the equation for $^0\mathbf{B}$ is given by the *unsteady* form of (2.11)

$$\frac{d\mathbf{B}^{(0)}}{dt} = -A\mathbf{B}^{(0)} + \mathbf{f}. \quad (3.4)$$

The solution of this equation is given by

$$\mathbf{B}^{(0)}(t) = (I - e^{-At})A^{-1}\mathbf{f}. \quad (3.5)$$

Next, we substitute (3.3) into (3.2) to obtain

$$\overline{B_p(x, t)C(x, 0, t)} = \overline{B}_p(t) - \text{Da } \overline{h(x)}\, B_p^{(0)}\frac{dB_\Sigma^{(0)}}{dt} + O(\text{Da}^2), \quad (3.6)$$

$$\overline{h(x)} = \frac{1}{x_{\max} - x_{\min}}\int_{x_{\min}}^{x_{\max}} \frac{3^{2/3}x^{1/3}}{\Gamma(2/3)}\, dx = \frac{3^{5/3}(x_{\max}^{4/3} - x_{\min}^{4/3})}{4\Gamma(2/3)(x_{\max} - x_{\min})}, \quad (3.7)$$

where we have used the spatial independence of the leading-order approximation. Then, one may use the relation

$$\text{Da } \overline{\mathbf{B}}(t) = \text{Da } \mathbf{B}^{(0)}(t) + O(\text{Da}^2) \tag{3.8}$$

to show (3.6) is equivalent to

$$\overline{B_p(x,t)C(x,0,t)} = \overline{B}_p \left(1 - \text{Da } \overline{h(x)} \frac{d\overline{B}_\Sigma}{dt} \right) + O(\text{Da}^2). \tag{3.9}$$

By proceeding in this manner we can derive a nonlinear set of ODEs of the form

$$\frac{d\overline{\mathbf{B}}}{dt} = M^{-1}(\overline{\mathbf{B}})(-A\overline{\mathbf{B}} + \mathbf{f}) + O(\text{Da}^2), \tag{3.10a}$$

$$\overline{\mathbf{B}}(0) = \mathbf{0}, \tag{3.10b}$$

where

$$M = I + \text{Da } N(\overline{\mathbf{B}}), \tag{3.10c}$$

$$N(\overline{\mathbf{B}}) = \overline{h(x)} \begin{pmatrix} {}_pK_a(R_p - \overline{B}_p) & {}_pK_a(R_p - \overline{B}_p) \\ (R_f - \overline{B}_f) & (R_f - \overline{B}_f) \end{pmatrix}, \tag{3.10d}$$

where A and $\mathbf{f}$ are as in (2.12). We refer to the set of Eqns. (3.10) as our *Effective Rate Constant* (*ERC*) equations, or our ERC approximation. We have also derived an ERC approximation for the wash phase of the experiment

$$\frac{d\overline{\mathbf{B}}}{dt} = M^{-1}(\overline{\mathbf{B}})(-\mathscr{D}\overline{\mathbf{B}}) + O(\text{Da}^2), \tag{3.11a}$$

$$\overline{\mathbf{B}}(0) = A^{-1}\mathbf{f}, \tag{3.11b}$$

where

$$\mathscr{D} = \begin{pmatrix} {}_fK_d & 0 \\ 0 & {}_pK_d \end{pmatrix}, \tag{3.11c}$$

and M, N are as in (3.10c) and (3.10d). The set of Eqs. (3.11) is derived from (2.7a)–(2.7b), (2.13), and (2.15) in the same manner that we derived (3.10) from (2.7) and (2.10d).

Since the ODE systems (3.10) and (3.11) are readily solved with a standard linear multistep or multistage formula (like an Adams-Bashforth method) these systems are far easier to solve numerically than their IDE counterparts. This simplicity and efficiency renders our ERC equations particularly attractive for data analysis, and thus can be used in iterative algorithms when fitting rate constants to reactions of the form (1.2).
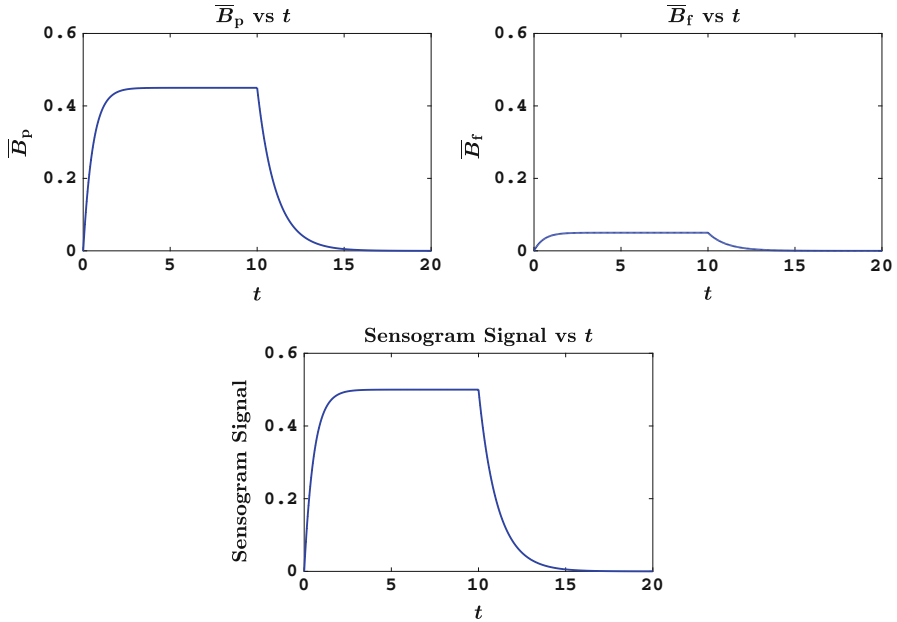
Fig. 4 The solution to our ERC Eqs. (3.10) and (3.11). From $0 \leq t \leq 10$ we have depicted the solution of injection phase (given by (3.10)), while the last 10 s correspond to the wash phase of the experiment (given by (3.11))

Table 2 Bounds for dimensionless parameters used in our numerical simulations are listed below, along with the aspect ratio ε, and representative values for the Reynolds number Re $= Vh^2/(vl)$ and Péclet number Pe $= Vh^2/(Dl)$

Dimensionless parameters		
Parameter	Description	Range
ε	Aspect ratio	0.02–0.05
Re	Reynolds number	0.019
Pe	Péclet number	4.80×10^2
Da	Damköhler number	0.02–150
$_fK_d$	Dimensionless dissociation rate constant in (1.2a)	1
$_pK_a$	Dimensionless association rate constant in (1.2b)	1–2
$_pK_d$	Dimensionless dissociation rate constant in (1.2b)	0.5–2
R_f	Ratio of free DNA receptors to total receptor concentration	0.1
R_p	Ratio of PCNA receptors to total receptor concentration	0.9

We have depicted the solutions of our ERC equations in Fig. 4; a range of dimensionless parameter values used in our simulations is given in Table 2. One may notice that $\overline{B}_f$ reaches a much lower chemical equilibrium than $\overline{B}_p$—this reflects the fact that free DNA receptors account for only ten percent of the total receptor population. Hence, in Fig. 4 we see that the sensogram signal is masked by ligand binding with

PCNA receptors. Therefore, to fit the rate constants $_fk_a$ and $_fk_d$ one could run two separate experiments: a first with *only* free DNA receptors on the sensor surface, and a second after depositing PCNA molecules onto the free DNA receptors. Doing an experiment with only free DNA molecules reduces our multiple-component system to a unimolecular one, and since unimolecular reaction kinetics in optical biosensors are well studied (see for example Edwards 1999, 2001; Edwards et al. 1999) this would allow one to estimate $_fk_a$ and $_fk_d$. With estimates for $_fk_a$ and $_fk_d$ in hand, one could then proceed to deposit PCNA molecules on the sensor surface and measure the rate constants $_pk_a$ and $_pk_d$.

It remains to show that our ERC equations are indeed accurate to $O(\text{Da}^2)$. To verify this, we develop a numerical approximation to our IDE system (2.7a)–(2.7b), using either (2.10d) or (2.15), and the appropriate initial conditions. We then use our numerical approximation to $B_p(x, t)$ and $B_f(x, t)$ to compute a numerical approximation to $\overline{B}_p(t)$ and $\overline{B}_f(t)$, and compare the latter with the solution of our ERC Eqs. (3.10), and (3.11).

3.2 Numerical method

Our numerical method is based upon the algorithms described Edwards and Jackson (2002), Evans and Edwards (2017). We outline our numerical method only for the injection phase of the experiment, since the wash phase requires only straightforward modifications. To find a numerical approximation to the solution of (2.7), (2.10d), we discretize the spatial interval [0, 1] into $N + 1$ equally spaced nodes $x_i = i\Delta x$, for $i = 0, \dots, N$, and discretize time by setting $t_n = n\Delta t$ for $n = 0, \dots$. Next, we must discretize the convolution integral (2.10d) and the time derivatives. Turning our attention to the former, we would like to spatially discretize (2.10d) with the trapezoidal rule, although there is a singularity in the integrand when $v = 0$. To handle the singularity we subtract and add

$$\frac{\partial B_\Sigma}{\partial t}(x - v, t)|_{v=0} \tag{3.12}$$

from the integrand of (2.10d). Doing so gives

$$C(x, 0, t) = 1 - \frac{\text{Da}}{3^{1/3}\Gamma(2/3)} \int_0^x \left[\frac{\partial B_\Sigma}{\partial t}(x - v, t) - \frac{\partial B_\Sigma}{\partial t}(x, t) \right. \\ \left. + \frac{\partial B_\Sigma}{\partial t}(x, t) \right] \frac{dv}{v^{2/3}}. \tag{3.13}$$

Since the last term of the integrand does not depend upon v, we may write (3.13) as

$$C(x, 0, t) = 1 - \frac{\text{Da}}{3^{1/3}\Gamma(2/3)} \left\{ \int_0^x \left[\frac{\partial B_\Sigma}{\partial t}(x - v, t) - \frac{\partial B_\Sigma}{\partial t}(x, t) \right] \frac{dv}{v^{2/3}} \right. \\ \left. + 3x^{1/3} \frac{\partial B_\Sigma}{\partial t}(x, t) \right\}. \tag{3.14}$$

With (2.10d) written as (3.14) we discretize $C(x, 0, t)$ in space using the trapezoidal rule

$$
\begin{aligned}
C(x_i, 0, t) = 1 - \frac{\mathrm{Da}}{3^{1/3}\Gamma(2/3)} &\left[\lim_{v \to 0} \frac{\Delta x}{2} \left(\frac{\partial B_\Sigma}{\partial t}(x_i - v, t) - \frac{\partial B_\Sigma}{\partial t}(x_i, t) \right) v^{-2/3} \right. \\
&\sum_{k=1}^{i-1} \Delta x \left(\frac{\partial B_\Sigma}{\partial t}(x_i - x_k, t) - \frac{\partial B_\Sigma}{\partial t}(x_i, t) \right) x_k^{-2/3} \\
&\left. \frac{\Delta x}{2} \left(\frac{\partial B_\Sigma}{\partial t}(0, t) - \frac{\partial B_\Sigma}{\partial t}(x_i, t) \right) x_i^{-2/3} + 3 x_i^{1/3} \frac{\partial B_\Sigma}{\partial t}(x_i, t) \right]
\end{aligned}
\tag{3.15a}
$$

when $i > 1$,

$$
\begin{aligned}
C(x_1, 0, t) = 1 - \frac{\mathrm{Da}}{3^{1/3}\Gamma(2/3)} &\left[\lim_{v \to 0} \frac{\Delta x}{2} \left(\frac{\partial B_\Sigma}{\partial t}(x_1 - v, t) - \frac{\partial B_\Sigma}{\partial t}(x_1, t) \right) v^{-2/3} \right. \\
&\left. \frac{\Delta x}{2} \left(\frac{\partial B_\Sigma}{\partial t}(0, t) - \frac{\partial B_\Sigma}{\partial t}(x_1, t) \right) x_1^{-2/3} \right],
\end{aligned}
\tag{3.15b}
$$

and

$$
C(x_0, 0, t) = 1.
\tag{3.15c}
$$

We expect that B_f and B_p are regular enough that

$$
\lim_{v \to 0} \frac{\Delta x}{2} \left(\frac{\partial B_\Sigma}{\partial t}(x_i - v, t) - \frac{\partial B_\Sigma}{\partial t}(x_i, t) \right) v^{-2/3} = 0.
\tag{3.16}
$$

We remark that at this point we have discretized (2.10d) in space only, so in this sense (3.15) may be viewed as a semi-discretization of (2.10d). Towards a full discretization of the convolution integral (2.10d) and our IDE system, we approximate the time derivatives as

$$
\frac{\partial B_j}{\partial t}(x_i, t_n) \approx \frac{\Delta B_{i,n+1}^j}{\Delta t} = \frac{B_{i,n+1}^j - B_{i,n}^j}{\Delta t},
\tag{3.17}
$$

where $j = \mathrm{p, f, \Sigma}$. In (3.17) $B_{i,n}^j$ is our discretized approximation to $B_j(x_i, t_n)$, and $\Delta B_{i,n+1}^j$ approximates the infinitesimal change in $B_j(x_i, t_{n+1})$. Although we have set $\Delta B_{i,n+1}^j = B_{i,n+1}^j - B_{i,n}^j$, as we shall show below $\Delta B_{i,n+1}^j$ is treated as a separate variable used to update $B_{i,n+1}^j$ at each time step.

The fully-discretized system is then given by

$$\frac{\Delta B^{\mathrm{p}}_{i,n+1}}{\Delta t} = {}_{\mathrm{p}}K_{\mathrm{a}}(R_{\mathrm{p}} - B^{\mathrm{p}}_{i,n})C_{i,n+1} - {}_{\mathrm{p}}K_{\mathrm{d}}B^{\mathrm{p}}_{i,n}, \qquad (3.18a)$$

$$\frac{\Delta B^{\mathrm{f}}_{i,n+1}}{\Delta t} = {}_{\mathrm{p}}K_{\mathrm{a}}(R_{\mathrm{f}} - B^{\mathrm{f}}_{i,n})C_{i,n+1} - {}_{\mathrm{p}}K_{\mathrm{d}}B^{\mathrm{f}}_{i,n}, \qquad (3.18b)$$

$$B_{i,0} = 0, \qquad (3.18c)$$

where

$$C_{i,n+1} = 1 - \frac{\mathrm{Da}}{3^{1/3}\Gamma(2/3)}\left[\sum_{k=1}^{i-1}\Delta x\left(\frac{\Delta B^{\Sigma}_{i-k,n+1}}{\Delta t} - \frac{\Delta B^{\Sigma}_{i,n+1}}{\Delta t}\right)x_k^{-2/3}\right.$$
$$\left.\frac{\Delta x}{2}\left(\frac{\Delta B^{\Sigma}_{0,n+1}}{\Delta t} - \frac{\Delta B^{\Sigma}_{i,n+1}}{\Delta t}\right)x_i^{-2/3} + 3x_i^{1/3}\frac{\Delta B^{\Sigma}_{i,n+1}}{\Delta t}\right] \qquad (3.18d)$$

for $i = 2, \ldots, N$, with straightforward modifications to $C_{i,n+1}$ when $i = 0$ or 1. Notice that this choice of $C_{i,n+1}$ in (3.18) renders our method only semi-implicit, rather than fully-implicit. Indeed, we could have chosen fully-implicit method by replacing all instances of $B^{j}_{i,n}$ with $B^{j}_{i,n+1}$ in (3.18a)–(3.18b), but a fully-implicit method introduces the expense and complication of solving a nonlinear system at each time step. On the other hand, we could have chosen an explicit method by replacing $B^{j}_{i,n+1}$ with $B^{j}_{i,n}$ in (3.18d).

To motivate our semi-implicit algorithm, observe the ν-dependence in the integrand of (2.10d) is only on $0 \le \nu \le x$. This enables us to use the *updated approximations* for $\partial B_j/\partial t(x_i, t_{n+1})$, rather than the previous approximation to $\partial B/\partial t(x_i, t_n)$, by discretizing (2.10d) as (3.18d) and marching our way downstream from x_0 to x_N at each time step. To wit, at a fixed time step t_{n+1} we start by taking $i = 0$ and using (3.18) to solve for $\Delta B^{j}_{0,n+1}$ in terms of $B^{j}_{0,n}$; note both $B^{j}_{0,n}$ and $\Delta B^{j}_{0,n}$ are known from the previous time step t_n. We then determine $B^{j}_{0,n+1}$ by taking $i = 0$ in our time-stepping formula

$$B^{\mathrm{p}}_{i,n+1} = B^{\mathrm{p}}_{i,n} + \frac{3}{2}\Delta B^{\mathrm{p}}_{i,n+1} - \frac{1}{2}\Delta B^{\mathrm{p}}_{i,n}, \qquad (3.19a)$$

$$B^{\mathrm{f}}_{i,n+1} = B^{\mathrm{f}}_{i,n} + \frac{3}{2}\Delta B^{\mathrm{f}}_{i,n+1} - \frac{1}{2}\Delta B^{\mathrm{f}}_{i,n}, \qquad (3.19b)$$

which is analogous to a second-order Adams-Bashforth method. Next we increment i to $i = 1$ and use $\Delta B^{j}_{0,n+1}$ in (3.18) to solve for $\Delta B^{j}_{1,n+1}$, which is possible since (3.18) is linear in $\Delta B^{j}_{i,n+1}$ thanks to the fact that our method is only semi-implicit. Then we use $\Delta B^{j}_{1,n+1}$ in (3.19) to determine $B^{j}_{1,n+1}$. We continue in this manner by iteratively incrementing i and marching our way downstream until we have determined $B^{j}_{i,n+1}$ for $i = 2, \ldots, N$. This process may be repeated for as many time steps as desired. To initialize our method, we replaced (3.19) with a single step of Euler's method.

With the above finite-difference approximation to $B_p(x, t)$ and $B_f(x, t)$, we may use the trapezoidal rule to compute an approximation to $\overline{B}_p(t)$ and $\overline{B}_f(t)$. At a given time-step t_n, our approximations to $\overline{B}_f(t_n)$ and $\overline{B}_p(t_n)$ take the form

$$\overline{B}_p(t_n) \approx \overline{B}_n^p = \frac{1}{x_{max} - x_{min}} \left(\frac{\Delta x}{2} B_{m,n}^p + \Delta x \sum_{i=m+1}^{M-1} B_{i,n}^p + \frac{\Delta x}{2} B_{M,n}^p \right), \quad (3.20a)$$

$$\overline{B}_f(t_n) \approx \overline{B}_n^f = \frac{1}{x_{max} - x_{min}} \left(\frac{\Delta x}{2} B_{m,n}^f + \Delta x \sum_{i=m+1}^{M-1} B_{i,n}^f + \frac{\Delta x}{2} B_{M,n}^f \right). \quad (3.20b)$$

In (3.20), the indices $i = m$ and $i = M$ correspond to the nodes $x_m = x_{min}$ and $x_M = x_{max}$. Therefore, our grid was chosen to align with these points to avoid interpolation errors.

We briefly comment on the temporal and spatial convergence properties of $\overline{B}_n^p$ and $\overline{B}_n^f$. These quantities converge at a rate of $O(\Delta t^2)$ in time, thanks to our second-order Adams-Bashforth method. Given the singular integrand in (2.10d), the issue of spatial convergence is more delicate and requires care. Our method converges at a rate of $O(Da \Delta x^2)$ when $Da \ll 1$, and $O(Da^2 \Delta x^{4/3})$ when $Da = O(1)$. We refer the interested reader to Evans and Edwards (2017) for more details, where the authors study the spatial and temporal convergence properties of this method applied to a different problem.

3.3 ERC verification

To test the accuracy of our ERC equations, we now compare the solutions of the ERC system (3.10) and (3.11) to the finite-difference approximation (3.20) for $\overline{B}_f(t)$ and $\overline{B}_p(t)$ generated from the more complicated integrodifferential equation system. The absolute difference between the solution of our ERC equations and our finite-difference approximation is depicted in Fig. 5, and the absolute difference between the corresponding sensogram readings is shown in Fig. 6. Upon inspecting the former, we see that the solutions to our ERC Eqs. (3.10) and (3.11) agree quite well with our finite-difference approximation. When $Da = 0.1$ the maximum absolute error is $O(10^{-4})$ for $\overline{B}_p$, and $O(10^{-5})$ for $\overline{B}_f$. Since available free DNA receptors account for only ten percent of the total receptor concentration, the absolute error for $\overline{B}_f$ is an order of magnitude smaller than the error for $\overline{B}_p$. Hence, we see the sensogram error depicted on the left in Fig. 6 is almost indistinguishable from the error associated with $\overline{B}_p$ in Fig. 5. Fortunately this does not pose an issue when measuring kinetic rate constants, since one can determine $_fk_a$ and $_fk_d$ through an experiment involving only free DNA molecules on the surface (as outlined in Sect. 3.1).

From the plot on the right in Fig. 6, it is evident that the solutions to our ERC Eqs. (3.10) and (3.11) agree with our finite-difference approximation not only for small Da, but for moderate Da as well. Though $Da = 0.45$, the absolute error reaches a maximum of only $O(10^{-3})$. These findings, which are summarized in Table 3, are consistent with the work of Edwards and Jackson (2002). In this work, the authors
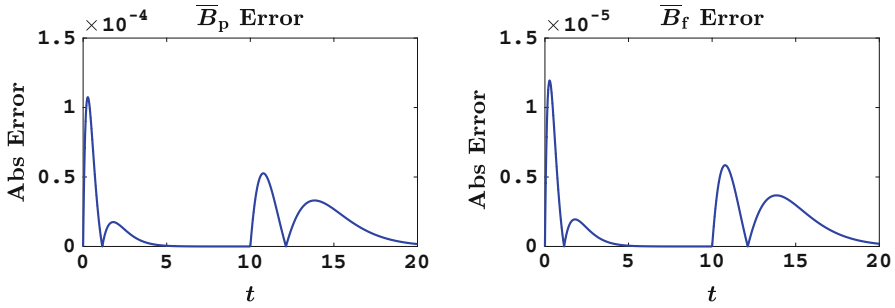
Fig. 5 Absolute error in $\overline{B}_p$ and $\overline{B}_p$ during both phases. From $t = 0$ to $t = 10$ we have depicted the absolute error during the injection phase (3.10), and from $t = 10$ to $t = 20$ we have depicted the absolute error during the wash phase (3.11). In both plots we have taken Da $= 0.1$ and all of the rate constants equal to one
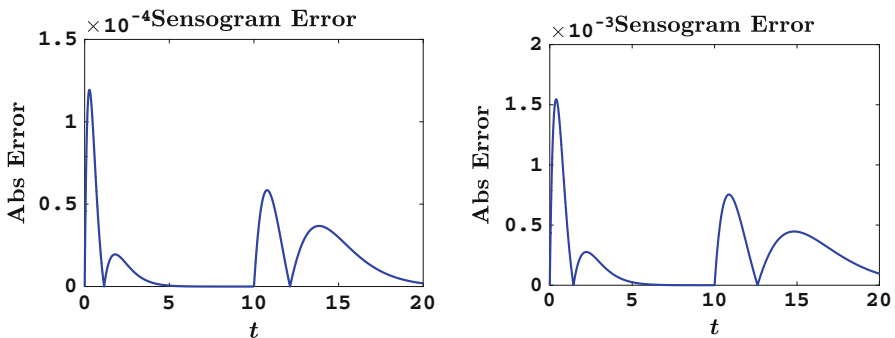
Fig. 6 Absolute error in sensogram during both phases. We have depicted the error in the signal resulting from (3.10) from $t = 0$ to $t = 10$, and the error in the signal resulting from (3.11) from $t = 10$ to $t = 20$. On the left we took Da $= 0.1$, and on the right we took Da $= 0.45$. In both, all rate constants were taken equal to one

Table 3 Summary of maximum absolute error during both phases

	$\overline{B}_f$	$\overline{B}_p$	S
Injection			
Da $= 0.1$	1.19×10^{-5}	1.07×10^{-4}	1.19×10^{-4}
Da $= 0.45$	1.53×10^{-4}	1.38×10^{-3}	1.53×10^{-3}
Wash			
Da $= 0.1$	5.85×10^{-6}	5.26×10^{-5}	5.85×10^{-5}
Da $= 0.45$	7.50×10^{-5}	6.75×10^{-4}	7.50×10^{-4}

demonstrate that a unimolecular analog of our multiple-receptor ERC equations can be used outside the range of which it is formally valid. Hence, motivated by Edwards and Jackson (2002), we tested the validity of our ERC approximations for a wider range of Da. The results are depicted in Fig. 7. To create the logarithmic plots in Fig. 7 we ran a series of simulations for different values of Da, from Da ≈ 0.02 to Da $= 150$, and measured the error at each value of Da by taking the maximum
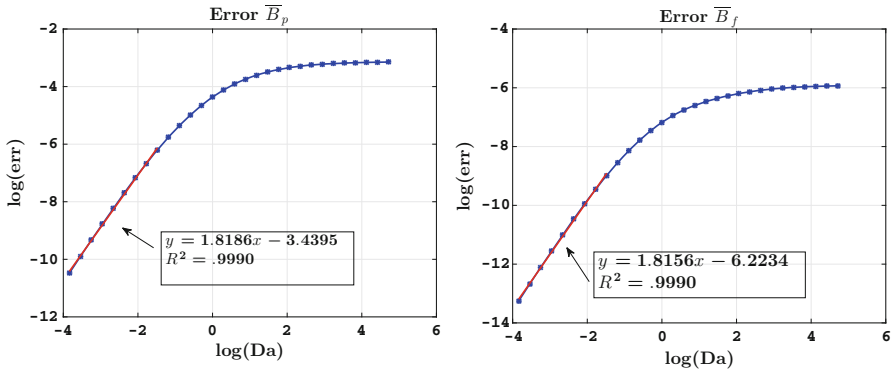
Fig. 7 *Left* the *red line* corresponds to the line $y = 1.8156x - 3.4394$. *Right* the *red line* corresponds to the line $y = 1.8156x - 6.2233$. In both plots, the rate constants were $_pK_a = 1$, $_pK_d = 1/2$, and $_fK_d = 1$. Similar results hold for the wash phase (color figure online)

absolute difference between the solution to ERC Eqs. (3.10) and our finite-difference approximation. Observe that the error starts off small, and increases at a rate which agrees favorably with our theoretical $O(\text{Da}^2)$ prediction. The error then reaches an asymptote corresponding to approximately a two percent absolute error. This indicates that our multiple-receptor ERC equations are also useful outside of the range which they are formally valid.

4 Conclusions

We developed and studied a mathematical model for surface-volume reactions in optical biosensors involving multiple-receptor types on the sensor surface. Motivated by current biosensor applications, we specifically considered the presence of both PCNA and free DNA receptors on the reacting surface. To quantify transport effects on such reactions, we modeled the biosensor experiment under consideration with a convection-diffusion equation coupled to a set of PDEs describing the surface reactions (1.2). Thanks to high Péclet number flow, transport effects are relevant only in a thin region near the surface and our PDE system reduces asymptotically to a nonlinear coupled set of IDEs for $\mathbf{B}(x, t) = (B_p(x, t), B_f(x, t))^T$ (a vector in $\mathbb{R}^2$ containing the concentration of ligand bound to PCNA receptors $B_p(x, t)$ and free DNA receptors $B_f(x, t)$. These IDEs are difficult to solve analytically, and a numerical solution does not readily lend itself to data analysis. Hence, we have further reduced these IDEs to a nonlinear set of ODEs, from which we can construct the sensogram signal (2.6).

Our ERC equations are formally valid only when $\text{Da} \ll 1$; i.e., when transport into the surface is much quicker than reaction and the two processes occur on different time scales. However, the results presented in Sect. 3.3 demonstrate that our ERC approximation agrees with our finite-difference approximation for $\text{Da} = O(1)$ and larger. Thus, our ERC approximation is useful not only in the reaction-limited parameter regime, but also in parameter regimes in which mass transport effects are thought to play a larger role. This flexibility, along with the fact that (3.10) and (3.11) are easily

solved with a standard numerical method for ODEs, render our ERC approximation particularly useful for data analysis. Though we have analyzed only two receptors herein, the vector formulations (3.10) and (3.11) readily extend to N receptors. We expect that the results discussed in Sect. 3.3 also generalize to N receptors, and future work may include a verification of this. We are also interested in quantifying other physical effects, such as: steric hindrance; random receptor orientation; or transport of the ligand molecules through a dextran gel layer, in which receptor sites are typically embedded.

References

Austin S (2009) Haemostasis. Medicine 37(3):133–136

Balgi G, Leckband DE, Nitsche JM (1995) Transport effects on the kinetics of protein-surface binding. Biophys J 68(6):2251–2260

Bertucci C, Piccoli A, Pistolozzi M (2007) Optical biosensors as a tool for early determination of absorption and distribution parameters of lead candidates and drugs. Comb Chem High Throughput Screen 10(6):433–440

Bird RB (2002) Transport phenomena. Appl Mech Rev 55(1):R1–R4

BIAcore T200 data file (2013) General electric life sciences, GE Healthcare Bio-Sciences AB, Björkgatan 30, 751 84 Uppsala

Cooper MA (2009) Sensor surfaces and receptor deposition. In: Cooper MA (ed) Label-free bioesnsors. Cambridge University Press, New York

de la Torre JG, Huertas ML, Carrasco B (2000) Calculation of hydrodynamic properties of globular proteins from their atomic-level structure. Biophys J 78(2):719–730

Edwards DA (1999) Estimating rate constants in a convection-diffusion system with a boundary reaction. IMA J Appl Math 63(1):89–112

Edwards DA (2001) The effect of a receptor layer on the measurement of rate constants. Bull Math Biol 63(2):301–327

Edwards DA (2004) Refining the measurement of rate constants in the BIAcore. J Math Biol 49(3):272–292

Edwards DA (2006a) Convection effects in the BIAcore dextran layer: surface reaction model. Bull Math Biol 68:627–654

Edwards DA (2006b) Convection effects in thin reaction zones: applications to BIAcore. SIAM J Appl Math 66(6):1978–1997

Edwards DA (2011) Transport effects on surface reaction arrays: biosensor applications. Math Biosci 230(1):12–22

Edwards DA, Goldstein B, Cohen DS (1999) Transport effects on surface-volume biological reactions. J Math Biol 39(6):533–561

Edwards DA, Jackson S (2002) Testing the validity of the effective rate constant approximation for surface reaction with transport. Appl Math Lett 15(5):547–552

Evans RM, Edwards DA (2017) Transport effects on multiple-component reactions in optical biosensors. Submitted

Friedberg EC (2005) Suffering in silence: the tolerance of DNA damage. Nat Rev Mol Cell Biol 6(12):943–953

Gervais T, Jensen KF (2006) Mass transport and surface reactions in microfluidic systems. Chem Eng Sci 61(4):1102–1121

Glaser W (1993) Antigen-antibody binding and mass transport by convection and diffusion to a surface: a two-dimensional computer model of binding and dissociation kinetics. Anal Biochem 213(1):152–161

Goldstein B, Coombs D, He X, Pineda AR, Wofsy C (1999) The influence of transport on the kinetics of binding to surface receptors: applications to cells and BIAcore. J Mol Recognit 12(5):293–299

Hu G, Gao Y, Li D (2007) Modeling micropatterned antigen-antibody binding kinetics in a microfluidic chip. Biosens Bioelectron 22(7):1403–1409

Jenkins J, Prabhakarpandian B, Lenghaus K, Hickman J, Sundaram S (2004) Fluidics-resolved estimation of protein adsorption kinetics in a biomicrofluidic system. Anal Biochem 331(2):207–215

Lagrée P-Y, Ivan-Fernolendt A (2004) Direct comparison of simplified models of surface reacting flows in flow chambers. Eur Phys J Appl Phys 26(2):133–143

Lehmann AR, Niimi A, Ogi T, Brown S, Sabbioneda S, Wing JF, Kannouche PL, Green CM (2007) Translesion synthesis: Y-family polymerases and the polymerase switch. DNA Repair 6(7):891–899

Liedberg B, Lundström I, Stenberg E (1993) Principles of biosensing with an extended coupling matrix and surface plasmon resonance. Sens Actuators B Chem 11(1):63–72

Myszka DG, He X, Dembo M, Morton Thomas A, Goldstein B, Goldstein B (1998) Extending the range of rate constants available from BIAcore: interpreting mass transport-influenced binding data. Biophys J 75(2):583–594

O'Shannessy DJ (1994) Determination of kinetic rate and equilibrium binding constants for macromolecular interactions: a critique of the surface plasmon resonance literature. Curr Opin Biotechnol 5(1):65–71

O'Shannessy DJ, Winzor DJ (1996) Interpretation of deviations from pseudo-first-order kinetic behavior in the characterization of ligand binding by biosensor technology. Anal Biochem 236(2):275–283

Plosky BS, Woodgate R (2004) Switching from high-fidelity replicases to low-fidelity lesion-bypass polymerases. Curr Opin Genet Dev 14(2):113–119

Raghaven M, Chen MY, Gastinel LN, Bjorkman PJ (1994) Investigation of the interaction between class I MHC-related F_c receptor and its immunoglobulin G ligand. Immunity 1(4):303–315

Rich RL, Cannon MJ, Jenkins J, Pandian P, Sundaram S, Magyar R, Brockman J, Lambert J, Myszka DG (2008) Extracting kinetic rate constants from surface plasmon resonance array systems. Anal Biochem 373(1):112–120

Rich RL, Myszka D (2011) Survey of the 2009 commercial optical biosensor literature. J Mol Recognit 24(6):892–914

Rich RL, Myszka DG (2009) Extracting kinetic rate constants from binding responses. In: Cooper MA (ed) Label-free biosensors. Cambridge University Press, New York

Schuck P (1996) Kinetics of ligand binding to receptor immobilized in a polymer matrix, as detected with an evanescent wave biosensor. I. a computer simulation of the influence of mass transport. Biophys J 70(3):1230

Schuck P (1997) Use of surface plasmon resonance to probe the equilibrium and dynamic aspects of interactions between biological macromolecules. Ann Rev Biophys Biomol Struct 26(1):541–566

Schuck P, Zhao H (2010) The role of mass transport limitation and surface heterogeneity in the biophysical characterization of macromolecular binding processes by SPR biosensing. In: Mol N, Fischer M (eds) Surface plasmon resonance. Methods in molecular biology (methods and protocols), vol 627. Humana Press

Svitel J, Boukari H, Van Ryk D, Willson RC, Schuck P (2007) Probing the functional heterogeneity of surface binding sites by analysis of experimental binding traces and the effect of mass transport limitation. Biophys J 92(5):1742–1758

Yarmush ML, Patankar DB, Yarmush DM (1996) An analysis of transport resistances in the operation of BIAcore; implications for kinetic studies of biospecific interactions. Mol Immunol 33(15):1203–1214

Zhuang Z, Johnson RE, Haracska L, Prakash L, Prakash S, Benkovic SJ (2008) Regulation of polymerase exchange between Polη and Polδ by monoubiquitination of PCNA and the movement of DNA polymerase holoenzyme. Proc Natl Acad Sci 105(14):5361–5366

Zumbrum M, Edwards DA (2014) Multiple surface reactions in arrays with applications to optical biosensors. Bull Math Biol 76(7):1783–1808